HYPOTHETICAL ACCIDENT SCENARIO MODELING FOR CONDENSED HYDROGEN STORAGE MATERIALS

Matthew R. Kesterson[1], David A. Tamburello[2], Jose A. Cortes-Concepcion, Charles W. James Jr.[3], and, Donald L. Anton[4]

[1] Applied Computational Engineering and Statistics, Savannah River National Lab, Aiken, 29808, U.S., matthew.kesterson@srnl.doe.gov
[2] Applied Computational Engineering and Statistics, Savannah River National Lab, Aiken, 29808, U.S., david.tamburello@srnl.doe.gov
[3] Material Science and Technology, Savannah River National Lab, Aiken, 29808, U.S., Charles.James@srs.gov
[4] Hydrogen and Alternative Energy Program, Savannah River National Lab, Aiken, 29808, U.S., Donald.Anton@srnl.doe.gov

ABSTRACT

Hydrogen is seen as an ideal energy carrier for stationary and mobile applications. However, the use of high energy density condensed hydrogen storage materials, such as NH_3BH_3, comes with risks associated with their high reactivity with water exposure and their decomposition products reactivity in air. To predict their behavior under these circumstances, idealized finite element models of hypothetical accident scenarios have been developed. Empirical thermodynamic calculations based on precise thermal gravimetric analysis (TGA) and calorimetric experiments have been performed in order to quantify the energy and hydrogen release rates and to quantify the reaction products resulting from water and air exposure.

NOMENCLATURE

AB – Ammonia Borane (NH_3BH_3)

TGA - Thermal Gravimetric Analysis

INTRODUCTION

Hydrogen is an ideal candidate for an energy carrier to replace fossil fuels. It has high energy content, is extremely abundant, and reduces the adverse effect to the environment seen with conventional fossil fuels. However, one of the leading challenges to the realization of the hydrogen economy is storage of the hydrogen. There has been significant work in the field of hydrogen storage in metal hydrides [1]; complex metal hydrides such as alanates [2-4], borohydrides [5-7], and amides [8-10]; and adsorbents [11-16]. While there is great interest in the potential use of these technologies for both stationary and mobile applications, there is only limited knowledge of the potential environmental reactivity risks associated with these materials.

Safe application of condensed hydrogen storage materials necessitates a quantitative understanding of their behavior under normal and off-normal conditions that may occur during application and handling. Hypothetical accident scenarios for hydride exposure are complex and numerous. Moreover, small variations in initial or boundary conditions for a particular scenario may result in very different hydride behavior. Thus, fundamental experiments, such as TGA and calorimetry, are modeled in order to quantify the energy, hydrogen release rate, and the reaction products resulting from water and air exposure. These fundamentals form the basis for more complex models of hypothetical accident scenarios.

The present study focuses on the release of powdered ammonia borane into ambient air. This work is part of a larger study with the objective to develop practical predictive capabilities for the behavior of condensed hydrogen storage materials exposed to ambient environmental conditions. Ultimately, this study seeks to identify those conditions most likely to result in hydride combustion events and the means for their mitigation. An understanding of the underlying causes for hydride combustion and the ability to predict the outcome of hypothetical accident scenarios will enable the development of appropriate, practical, effective, and commercially acceptable safety procedures and systems.

MATERIAL AND EXPERIMENTAL CONSIDERATIONS

Ammonia borane (Aldrich), with 90% purity, was used as received. Thermal gravimetric analyses, TGA, were done on a Pelkin-Elmer – Pyris 1 TG-RGA to determine the thermal stability and the hydrogen storage capacity of the materials. This instrument was placed inside of an argon-filled glove box so that samples could be analyzed with virtually no exposure to air and moisture. Additionally, to quantify the heat released through contact with dry and humidified air, further analyses were performed in a Setram C80 calorimeter with a gas flow cell. The heat flow (mW) was normalized with respect to the mass of hydride and plotted versus time. Controlled humid-air reaction measurements were initially set at 40 ^{o}C and 30% relative humidity. The temperature was increased to 260 ^{o}C at a ramp rate of 0.5 ^{o}C/min. For these measurements, the calorimeter was equipped with a flow cell with air as the carrier gas at a flow rate of 10 mL/min reacting with 5-10 mg of solid material. Calorimetry experiments were also performed in argon environment for further comparison/validation between experimental setups.

AB PARAMETERS

AB Kinetics

In order to develop simulations for the ammonia borane system, expressions for the reaction rate equations as well as values for the parameter therein needed to be determined. As a starting point, the dehydrogenation of AB was modelled by four reactions. Reactions 1 and 2 are a dehydrogenation to NH_2BH_2 and borazine, respectively, where all non-hydrogen products are assumed to only be borazine.

$$NH_3BH_3 \rightarrow NH_2BH_2 + H_2 \quad (1)$$

$$NH_3BH_3 \rightarrow {}^{1}/_{3}\,(BH)_3(NH)_3 + 2H_2 \quad (2)$$

The second set of reactions release additional hydrogen and borazine (reactions 3 and 4).

$$NH_2BH_2 \rightarrow NHBH + H_2 \quad (3)$$

$$NH_2BH_2 \rightarrow {}^{1}/_{3}\,(BH)_3(NH)_3 + H_2 \quad (4)$$

Reactions (1) and (2) were assumed to happen simultaneously and, therefore, employ the same rate constants. Each reaction rate was multiplied by the fraction of borazine or NH_2BH_2 that is formed. These fractions were determined based on mass balance fits to the TGA data, as shown in Figure 1. The same constraints are applied to the reactions (3) and (4).

$$R_{1,2} = k_{1,2} * C_{AB} \quad (5)$$

$$R_{3,4} = k_{3,4} * C_{NH2BH2} \quad (6)$$

It was further assumed that the reactions could be modelled by an Arrhenius equation (Eq. 7).

$$k(T) = A * \exp(-Ea/RT) \quad (7)$$

where: Ea = Activation Energy
A = frequency factor
T = Absolute Temperature

In order to fully model the AB system, the heat released during the dehydrogenation steps was needed. Based on literature [17,19,20,21], the heat of reaction for the first set of reactions ranges between -9 and -21.7 kJ/mol_{AB}, whereas the second set of reactions yields a heat of reaction between -15 to -24 kJ/mol_{AB}.

To obtain initial estimates for Ea and A, a sum of squares fit was performed against the experimental TGA data and the reaction rate equations using a small *dt* value. The resulting values were then used in a COMSOL Multiphysics® model and tuned until the model results achieved a close approximation to the experimental results, as shown in Figure 1. This method yielded the parameters to the Arrhenius equation shown in Table 1. The heat of reaction for sets (1,2) and (3,4) were obtained from existing literature data [17,19,20,21] as well as calorimetry experiments. The heats of reaction used in the simulations were -13.7 kJ/mol for reactions (1) and (2) and -8.9 kJ/mol for reactions (3) and (4).

Table 1- Rate Parameters for the dehydrogenation of AB

	Reactions 1 and 2	**Reactions 3 and 4**
Ea (KJ/mol)	128	76
A (1/s)	$5x10^{11} * 7.67x10^{-23} * exp^{(0.1573*T)}$	$1x10^{6}$
Borazine Yield (mol %)	14	41

Material Properties

As inputs to the COMSOL Multiphysics® model, the physical properties of AB, the properties of the gas phase, as well as that of the apparatus are needed. For all of the TGA runs, the simulations were conducted in an atmosphere of Argon. The relevant properties of Argon are shown in Table 2. Note that unless otherwise stated, all temperatures are reported in Kelvin.

Table 2 - Material Properties for Argon

Property	Value	Units
Heat Capacity [18]	20.786	[J/mol/K]
Thermal Conductivity [18]	$17.72x10^{-3}$	[W/m/K]

Additionally, models to simulate the calorimetry experiments were created. For these simulations an air atmosphere was used. In order to obtain a more accurate simulation the following material properties (Tables 3-5) for the gas phase and AB were used.

Table 3 - Material Properties for Air

Property	Value	Units
Heat Capacity	0.1608*T + 951.31	[J/kg/K]
Thermal Conductivity	$4.217562x10^{-3} + 7.1997361x10^{-5}$*T	[W/m/K]

Table 4 - Material Properties for Hydrogen

Property	Value	Units
Heat Capacity [18]	14.75	[J/g/K]
Thermal Conductivity [18]	0.2	[W/m/K]
Diffusion Coefficient for Hydrogen in Air	$-1.7842333x10^{5} + 1.9078581x10^{7}$*T + $4.2956672 x10^{10}$*T^2	[m^2/s]

Table 5 - Material Properties for AB

Property	Value	Units
Heat Capacity	$-2.015498 + 0.012129193*T + 76753.026/T^2$	[J/g/K]
Thermal Conductivity	-44.482278 + 0.19512749*T	[W/m/K]
Density	0.765	[g/cm^3]
Porosity	0.5	

RESULTS AND DISCUSSION

Computer models of both the TGA and calorimeter systems were created using COMSOL Multiphysics® version 3.5a. COMSOL Multiphysics® is a commercially available finite element software package. COMSOL Multiphysics® is divided into numerous specialized submodules (such as Acoustics, CFD, Heat Transfer, or Structural Mechanics modules) with specialized equations tailored to solving specific problems. In addition, COMSOL Multiphysics® includes the capability to write user-defined equations (algebraic and/or differential) in order to extend the software capabilities beyond its built-in equations. For the purposes of this work, the Chemical Engineering module was used. The Chemical Engineering module includes the reaction rate diffusion and convection equations necessary to track the changes in species concentration during the dehydrogenation of AB. This module also includes equations to calculate heat transfer due to conduction, convection, and radiation while also incorporating variable density flow using Navier-Stokes to calculate velocities within the gas phase.

TGA

Figure 2 shows the geometry of the AB TGA simulations. For the TGA, a 2D axisymmetric model was created with an overall sample chamber height of 5 mm, a sample chamber radius of 2 mm, and a sample height of 1 mm. The mesh consists of 700 quadrilateral mesh elements. Corresponding to the laboratory TGA experiments, the base of the simulated TGA was initialized to 40 ºC and then ramped to 250 ºC at a rate of 0.8 ºC/min. The results of the simulation show a close approximation to the experimental results as shown in Figure 1.

Calorimetry

The geometry for the calorimeter model (as shown in Figure 3) was more complicated than the TGA geometry. For this model, the dimensions and material of an actual sample cell were used. The calorimeter used in the experimental measurements was a Setram C80 calorimeter with a gas flow cell. The sample cell consists of a stainless steel housing approximately 1/16 inch thick with a gas flow tube in the center (Tube wall thickness 1/32 inch). The calorimeter mesh consists of 1439 triangular mesh elements with an additional 200 quadrilateral mesh elements. The top boundary of the gas flow tube is modeled as an outlet boundary condition with a pressure of 1 atm. For the simulated calorimetry runs, the walls, in addition to the base, were set to 40 ºC and ramped to 260 ºC at a rate of 0.5 ºC/min. Figure 4 presents the comparison between the simulation and the experimental results.

Accident Scenarios

As a further extension of the model parameters, two different COMSOL Multiphysics® models of hypothetical accident scenarios were generated based on the previous fundamental models. The first scenario had a heat source located above the sample, while the second scenario had the heat source located below the sample. Both scenarios assume that a 50 g sample of AB is dropped onto the ground, with the sample shape following a Gaussian distribution, as shown in Figure 5. Radiative heat transfer is applied to the surface of the sample based on the sample temperature and the temperature of the overhead surface.

For the first accident scenario, a single height of 0.1 m (~4 inches) above the mound of AB was chosen for the heat source. Heat sources located higher above (farther from) the mound of AB should yield a slower reaction rate for a given heat source temperature. Therefore, the 0.1 m case should be the most reactive and, therefore, a worst case scenario. Several above heat source temperatures (225 ^{o}C, 250 ^{o}C, 275 ^{o}C, and 300 ^{o}C) were simulated and their results are shown in Figures 6 – 9. As these figures show, the first dehydrogenation reaction of AB occurs relatively quickly with a heated surface of 250 ^{o}C and above. The second reaction is less intense and is not shown to go to completion after an hour of exposure to the heated surface. At surface temperatures above 300 ^{o}C, the reaction occurs at such a high rate that it causes instabilities within the simulation, which reduce the simulation timestep by several orders of magnitude. If allowed to continue, the simulation would take weeks or longer to reach the final time.

In Figures 10 and 11, the temperature and hydrogen profiles, respectively, are shown for a simulation time of 15 minutes with an above surface temperature of 275 ^{o}C. As the reaction progresses, hydrogen and borazine (at a higher temperature than the ambient air) emanates from the hydride forming vortical structures that advect out of the simulation domain without appreciable accumulation.

In the second hypothetical accident scenario, the mound of AB falls onto a heated surface. This scenario offers a unique situation. For the above heating accident scenarios, the heat and hydrogen are able to dissipate into the ambient relatively easily. With the hydride pile on top of the heated surface, the hydride pile acts as an insulator and flow inhibitor due to its poor thermal conductivity and low permeability, respectively. Because of these impediments, heated surface temperatures greater than 125 ^{o}C cause the first reaction to progress so rapidly that the simulation decreases the timestep by several orders of magnitude. The simulation, if allowed to continue, would take weeks or longer to reach the final time. Figures 12 and 13 show the temperature and hydrogen plots, respectively, for a base heated surface temperature of 120 ^{o}C.

As seen in Figures 11 and 13, the concentration of hydrogen increases rapidly for the bottom surface heating compared to the top surface heating. In addition, a high pressure region forms within the sample corresponding to the high hydrogen concentration location. Due to the rigid nature of the model, the geometry cannot change even though the calculated pressure would be high enough to dislodge some of the media from the pile. This rigidity does not allow the model to predict any shape alterations or foaming as seen in the laboratory experiments. However, these high pressure regions (due to rapid hydrogen release) may be the precursor to the foaming behavior seen in the experiments. Through further analysis (outside the scope of the present study), the connection between these high pressure regions and foaming could be proven making the prediction of foaling behavior a possibility.

CONCLUSIONS

The models created to simulation the dehydrogenation reactions for ammonia borane yielded similar results to the experimental results from thermal gravimetric analysis and calorimetry. Results from these simulations of fundamental experiments formed the basis for hypothetical accident scenario simulations of a mound of AB exposed to a heat source (either above the mound or below it) in an air environment.

These hypothetical accident scenarios were used to find the bounding heating conditions for a mound of AB heated from below (120 ^{o}C) and heated from above (300 ^{o}C) in which the first dehydrogenation reaction progresses so rapidly that the simulation decreases the calculation timestep several orders of magnitude, prohibiting results from the simulation to be obtained in a reasonable time. Below these temperatures and within the simulation time allotted, the first set of reactions proceeded to completion while the second set of reactions (in all cases) was shown to be appreciably slower than the first set of reactions, taking multiple hours to complete. In addition, the hypothetical accident scenario models showed pressure spikes (due to rapid hydrogen release) within the mound of material that could be the

precursor to foaming shown experimentally. With further study, this connection to foaming could lead to predictive capabilities.

ACKNOWLEDGEMENTS

This work was funded under the U.S. Department of Energy (DOE) Hydrogen Safety, Codes, & Standards Program managed by Dr. Ned Stetson

FIGURES

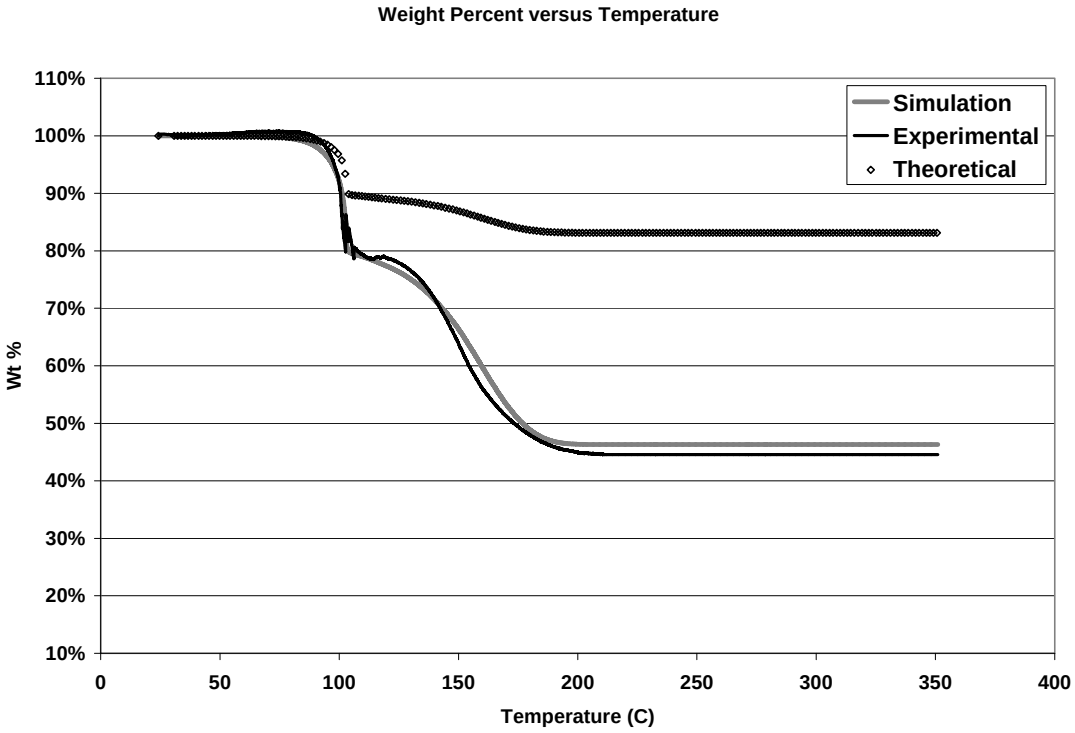

Figure 1 - Simulation, TGA experimental data, and theoretical mass reduction with temperature.

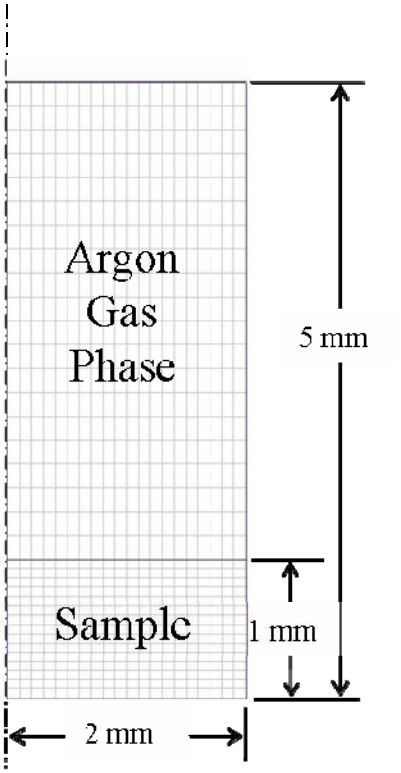

Figure 2 - COMSOL Multiphysics® subdomains for the TGA simulations involving AB.

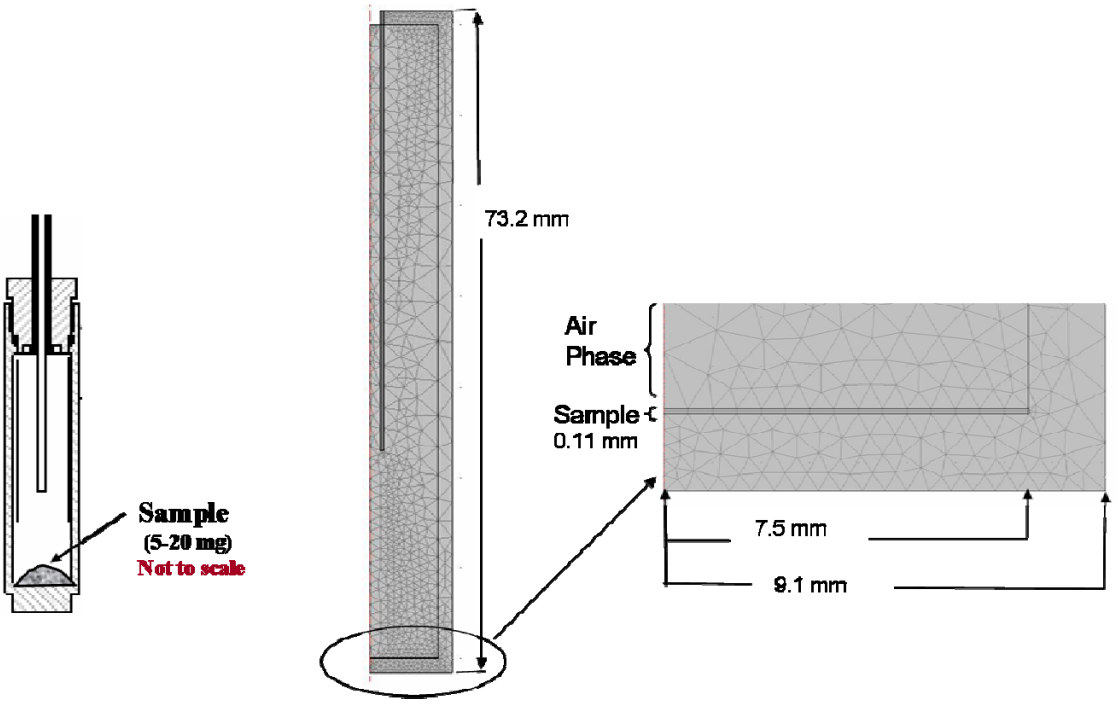

Figure 3 – Basic sketch and COMSOL Multiphysics® subdomains for the calorimetry simulations involving AB.

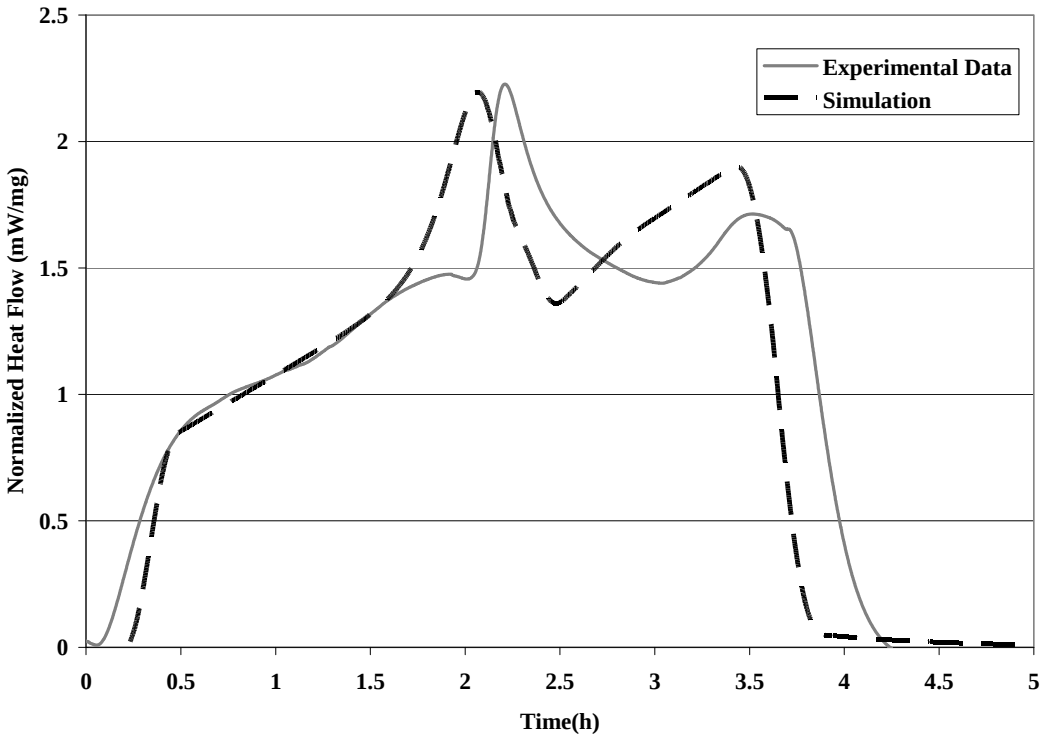

Figure 4 - Normalized heat flow with time for simulation and calorimetry experimental data.

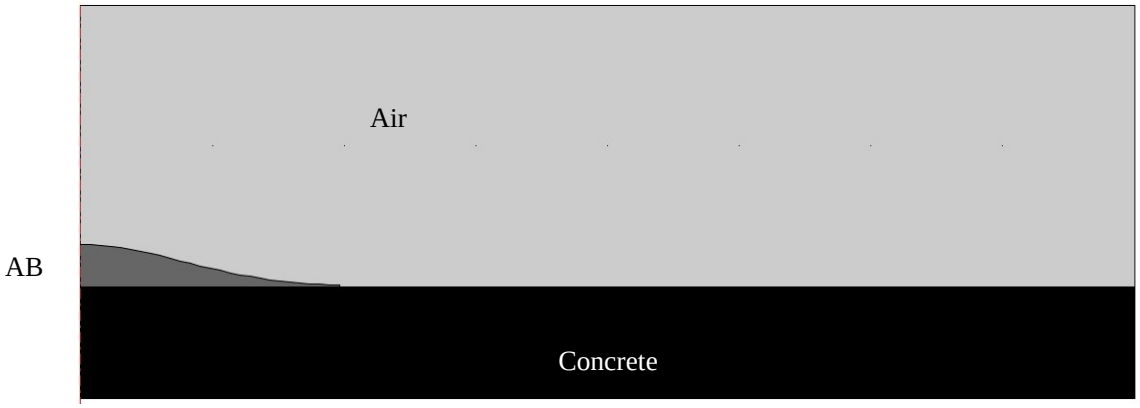

Figure 5 - COMSOL Multiphysics® subdomains for the hypothetical accident scenarios involving AB.

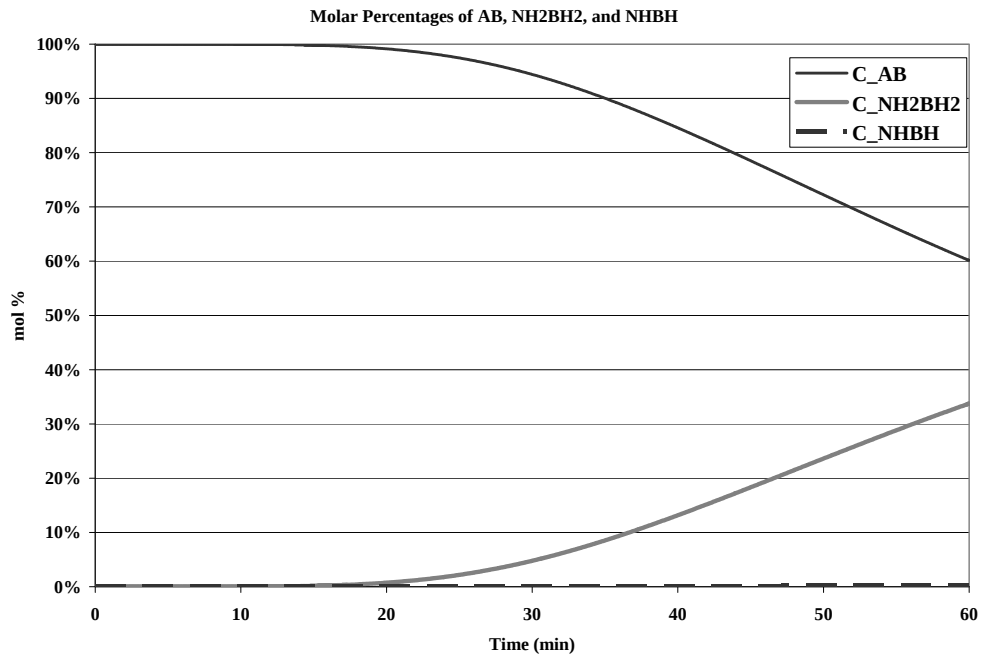

Figure 6 - Mole fraction plot of AB, NH_2BH_2, and NHBH for an above heat temperature of 225ºC.

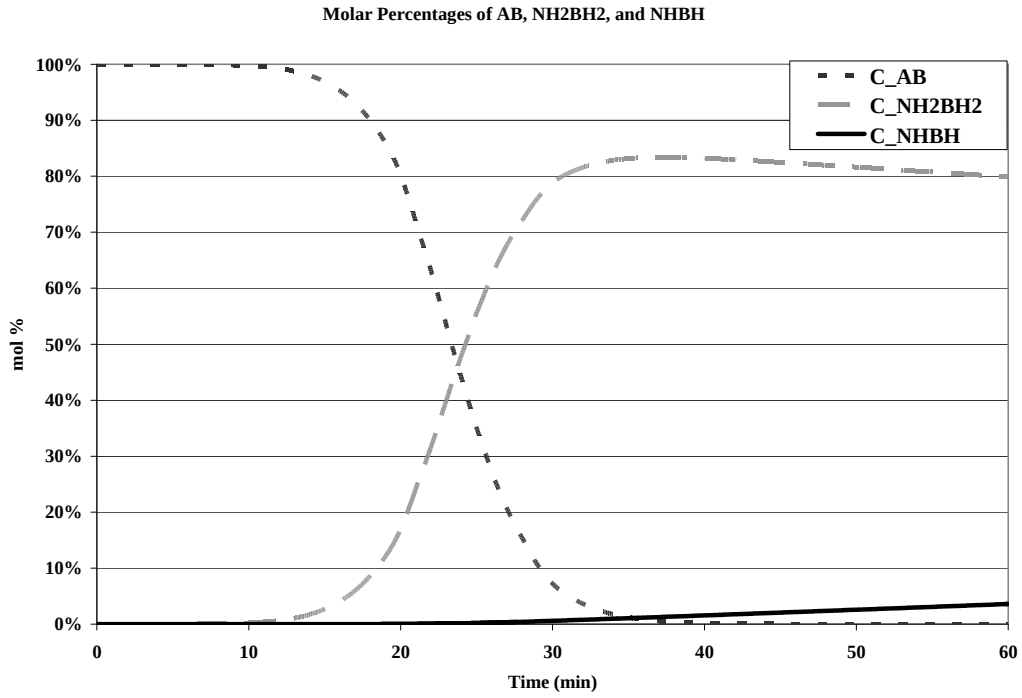

Figure 7 - Mole fraction plot of AB, NH2BH2, and NHBH for an above heat temperature of 250ºC.

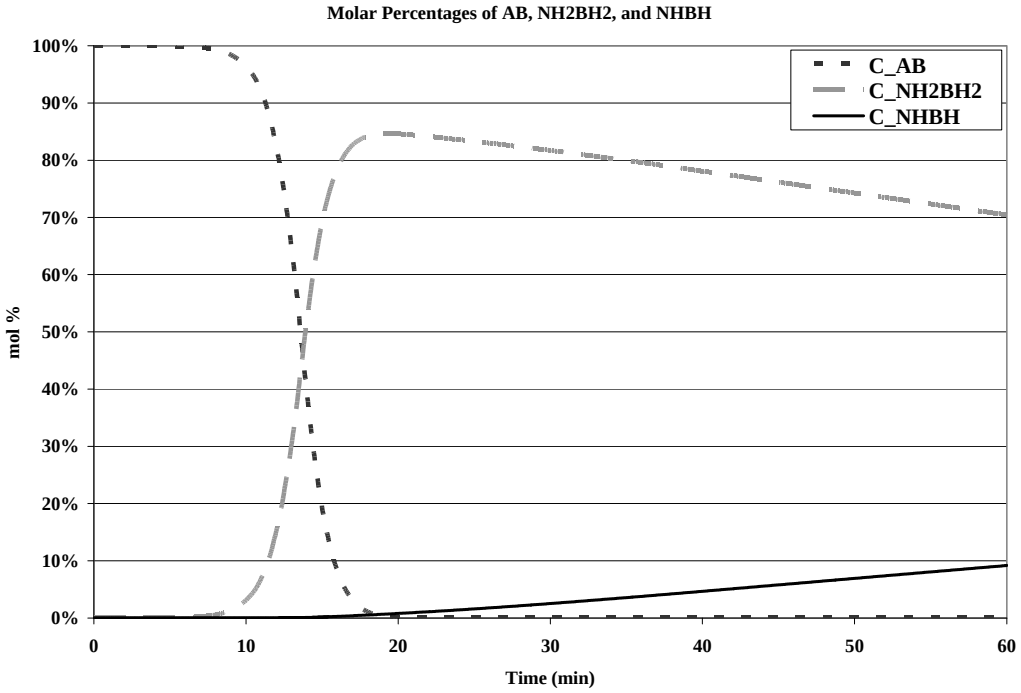

Figure 8 - Mole fraction plot of AB, NH2BH2, and NHBH for an above heat temperature of 275ºC.

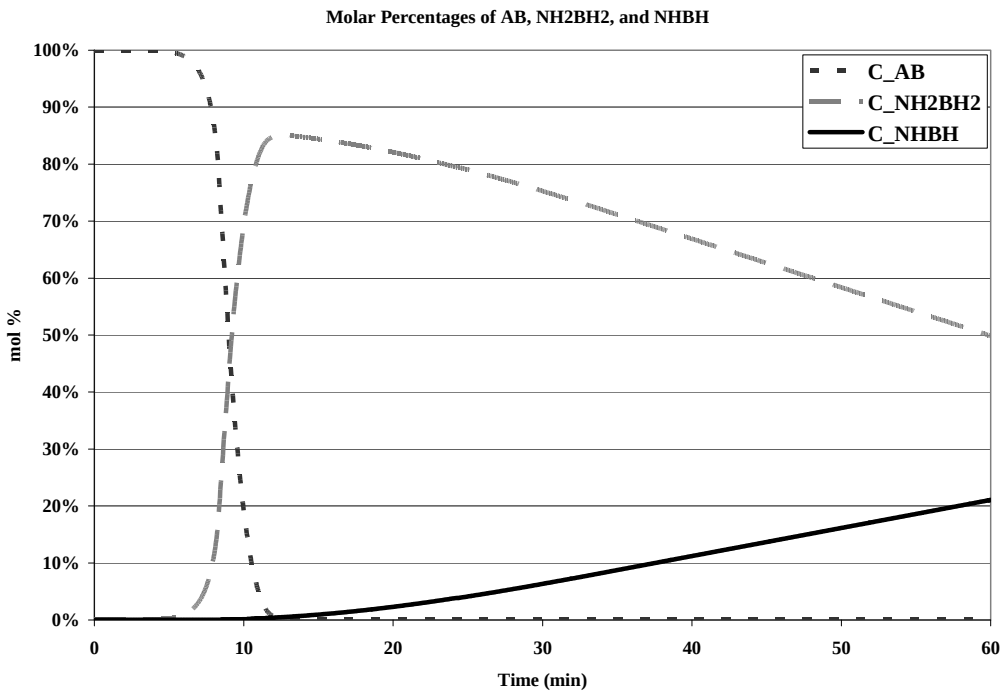

Figure 9 - Mole fraction plot of AB, NH2BH2, and NHBH for an above heat temperature of 300ºC.

Figure 10 – Temperature plot (ºC) during first dehydrogenation reaction of AB.

Figure 11 - Hydrogen concentration (mol/m^3) during the first dehydrogenation reaction of AB.

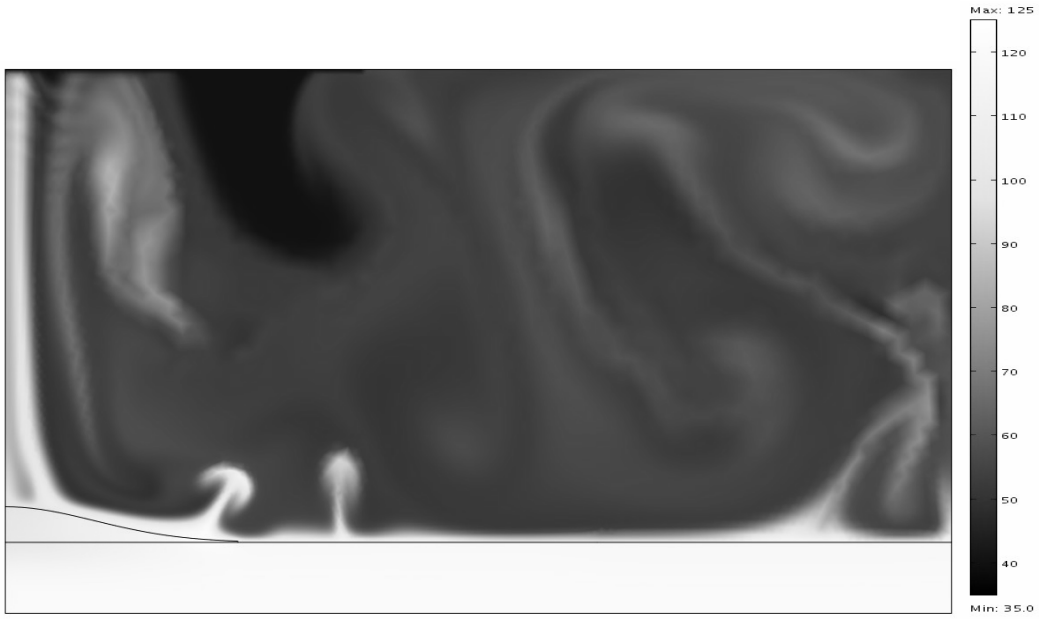

Figure 12 - Temperature plot (ºC) during first dehydrogenation reaction of AB.

Figure 13- Hydrogen concentration (mol/m^3) during the first dehydrogenation reaction of AB.

REFERENCES

1. Sakintuna B, Lamari-Darkrim F, Hirscher M. Metal hydride materials for solid hydrogen storage: A review. International Journal of Hydrogen Energy 2007;32:1121.
2. Anton DL. Hydrogen desorption kinetics in transition metal modified NaAlH4. Journal of Alloys and Compounds 2003;356-357:400.
3. Walters RT, Scogin JH. A reversible hydrogen storage mechanism for sodium alanate: the role of alanes and the catalytic effect of the dopant. Journal of Alloys and Compounds 2004;379:135.
4. Bogdanovic B, Felderhoff M, Germann M, Härtel M, Pommerin A, Schüth F, Weidenthaler C, Zibrowius B. Investigation of hydrogen discharging and recharging processes of Ti-doped NaAlH4 by X-ray diffraction analysis (XRD) and solid-state NMR spectroscopy. Journal of Alloys and Compounds 2003;350:246.
5. Züttel A, Wenger P, Rentsch S, Sudan P, Mauron P, Emmenegger C. LiBH4 a new hydrogen storage material. J Power Sources 2003;118:1.
6. Züttel A, Rentsch S, Fischer P, Wenger P, Sudan P, Mauron P, Emmenegger C. Hydrogen storage properties of LiBH4. Journal of Alloys and Compounds 2003;356-357:515.
7. Au M. Hydrogen Storage Reversibility of LiBH4 Based Materials. Presentation at the Fall 2005 MRS Meeting, Boston, MA, 2005.
8. Pinkerton FE. Decomposition kinetics of lithium amide for hydrogen storage materials. Journal of Alloys and Compounds 2005;400:76.
9. Song Y, Yang R. Decomposition mechanism of magnesium amide Mg(NH2)2. Int J Hydrogen Energy 2009;34:3778.
10. Lu J, Choi YJ, Fang ZZ, Sohn HY. Effect of milling intensity on the formation of LiMgN from the dehydrogenation of LiNH2-MgH2 (1:1) mixture. J Power Sources;195:1992.
11. Chen X-W, Su DS, Hamid SBA, Schlogl R. The morphology, porosity and productivity control of carbon nanofibers or nanotubes on modified activated carbon. Carbon 2007;45:895.

12. Dillon AC, Gilbert, K.E.H., Parilla, P.A., Horbacewicz, C., Alleman, J.L., Jones, K.M., Heben, M.J. Hydrogen Storage in Carbon Single-wall Nanotubes. Hydrogen, Fuel Cells, and Infrastructure Technologies 2003.
13. Schlichtenmayer M, Streppel B, Hirscher M. Hydrogen physisorption in high SSA microporous materials - A comparison between AX-21_33 and MOF-177 at cryogenic conditions. International Journal of Hydrogen Energy;36:586.
14. Yürüm Y, Taralp A, Veziroglu TN. Storage of hydrogen in nanostructured carbon materials. International Journal of Hydrogen Energy 2009;34:3784.
15. Züttel A, Sudan P, Mauron P, Kiyobayashi T, Emmenegger C, Schlapbach L. Hydrogen storage in carbon nanostructures. International Journal of Hydrogen Energy 2002;27:203.
16. Thomas KM. Hydrogen adsorption and storage on porous materials. Catalysis Today 2007;120:389.
17. Hirscher, M., Handbook of Hydrogen Storage: New Materials for Future Energy Storage, 2010, Wiley-VCH, Weinheim
18. Lide, D.R., CRC Handbook of Chemistry and Physics, 74th Edition, CRC Press, 1993, Boca Raton
19. Rassat , S.D., Aardahl, C.L., Autrey, T., and Smith, R.S., Thermal Stability of Ammonia Borane: A Case Study for Exothermic Hydrogen Storage Materials, Energy Fuels 2010, 24, 2596–2606
20. Mohajeri, N., Raissi , T., Ramasamy, K., Adebiyi, O., Bokerman, G., Ammonia-Borane Complex for Hydrogen Storage, NASA/CR 2009-215441,Florida Solar Energy Center
21. Gutowsk, M., and Autrey, T., Computational Studies of Boron/Nitrogen and Aluminum/Nitrogen Compounds for Chemical Hydrogen Storage, Prepr. Pap.-Am. Chem. Soc., Div. Fuel Chem. 2004, 49 (1), 275-276